Deep learning detection of dynamic exocytosis events in fluorescence TIRF microscopy

Hugo Lachuer[1*], Emmanuel Moebel[2*], Anne-Sophie Macé[3], Arthur Masson[2], Kristine Schauer[4+], Charles Kervrann[2+]

1: Université de Paris, CNRS, Institut Jacques Monod, 75013 Paris, France

2: SAIRPICO team, Centre Inria de l'Université de Rennes, INSERM-U1143, Institut Curie, PSL Research University, Campus Universitaire de Beaulieu, Rennes Cedex, France.

3: Cell and Tissue Imaging Facility (PICT-IBiSA), Institut Curie, PSL Research University, Paris, France.

4: Tumor Cell Dynamics Unit, Inserm U1279 Gustave Roussy Institute, Université Paris-Saclay, Villejuif 94800, France.

*: These authors contributed equally

+: Corresponding authors

Abstract

Segmentation and detection of biological objects in fluorescence microscopy is of paramount importance in cell imaging. Deep learning approaches have recently shown promise to advance, automatize and accelerate analysis. However, most of the interest has been given to the segmentation of static objects of 2D/3D images whereas the segmentation of dynamic processes obtained from time-lapse acquisitions has been less explored. Here we adapted DeepFinder, a U-net originally designed for 3D noisy cryo-electron tomography (cryo-ET) data, for the detection of rare dynamic exocytosis events (termed ExoDeepFinder) observed in temporal series of 2D Total Internal Reflection Fluorescent Microscopy (TIRFM) images. ExoDeepFinder achieved good absolute performances with a relatively small training dataset of 60 cells/~12000 events. We rigorously compared deep learning performances with unsupervised conventional methods from the literature. ExoDeepFinder outcompeted the tested methods, but also exhibited a greater plasticity to the experimental conditions when tested under drug treatments and after changes in cell line or imaged reporter. This robustness to unseen experimental conditions did not require re-training demonstrating generalization capability of ExoDeepFinder. ExoDeepFinder, as well as the annotated training datasets, were made transparent and available through an open-source software as well as a Napari plugin and can directly be applied to custom user data. The apparent plasticity and performances of ExoDeepFinder to detect dynamic events open new opportunities for future deep-learning guided analysis of dynamic processes in live-cell imaging.

Main

Technological improvements in imaging accelerate the amount of acquired data. This situation requires new methods to automatically extract the tremendous quantity of information present in them. It is clearly established that Deep-Learning-based image segmentation methods, and especially U-net[1], surpass conventional techniques and exhibit a remarkable generalisation capacity[1,2]. However, most of the studies are restricted to the segmentation of static biological objects. Deep-Learning-methods are rarely applied to dynamic processes[3] while several model-based methods have been developed in the past decades[4–7]. Here we focus on the supervised Deep-Learning-assisted detection of rare dynamic exocytosis events (< 1 event per frame in average) in videos. Exocytosis is the fusion of an intracellular vesicle with the plasma membrane to release its content. Many conventional methods of exocytosis detection have been already published[8–23] including a deep-learning strategy[24]. These methods detect exocytosis events visualized by an exocytic reporter protein tagged with a pH-sensitive fluorophore[25] imaged in Total Internal Reflection Fluorescence Microscopy (TIRFM). In general, a sudden peak of fluorescence intensity (termed "puff") followed by an exponential decay of the signal (**F1A**) is detected. Unfortunately, these methods are often poorly evaluated on benchmark datasets and are not publically available.

Here we present an adaptation of DeepFinder[26] (**see Methods**), a U-net deep-learning method, for the detection of exocytosis events in large 2D+Time volumes. DeepFinder was originally developed for the identification of macromolecules in 3D noisy cellular cryo-tomograms (cryo-ET) and is considered as a top-rank method, confirmed in several SHREC challenges[27]. To train "ExoDeepFinder" we took advantage of our recently published large dataset[28] monitoring lysosomal exocytosis events via imaging of VAMP7-pHluorin by TIRFM. The coordinates of all exocytosis events were manually annotated by a single expert based on the characteristic "puff" signature (**F1A-B and movie S1**). Because DeepFinder performances for cryo-ET segmentation substantially increased thanks to a multi-class strategy, we applied a similar approach here: We combined manual annotations of exocytosis events with automatic algorithm-generated annotations of docked vesicles at the plasma membrane[29] that form bright foci without fusion with the plasma membrane (**see Methods**) (**Fig 1C**).

Furthermore, we evaluated detection performance as a function of the "Signal-to-Background Ratio" (SBR). We defined the SBR as a ratio between the local fluorescence intensity F after vesicle fusion with the plasma membrane and the fluorescence intensity F_0 before this peak, *i.e.* $SBR = F/F_0$. We constituted a dataset of 120 TIRFM movies (for a total of 20 567 exocytosis events) of 1001 frames (about 6 minutes) that we divided into three groups based on their average SBR (**F1D**). Then we split randomly each SBR group into two sub-groups, one dedicated to training of the network and the other one to its evaluation (**F1D**). We made our dataset entirely available (**see supplementary**).

We trained ExoDeepFinder on the three sub-datasets (low, medium, and high SBR values), on the combination of these three datasets (Subsets A to D) (**Table S1**) and on the full training dataset (i.e. 60 movies). ExoDeepFinder performances for each training set were evaluated in terms of F1-score, Recall and Precision over the whole inference dataset (*i.e.* 60 movies). As commonly observed for neural network approaches, the best performances were achieved with the training over the full training dataset with 67.64% for F1, 70.07% for Recall and 68.75% for Precision (**Table 1**). Moreover, we compared these performances to the two unsupervised, conventional exocytosis detection methods that are publically available i) ExoJ[22] and ii) ADAE GUI[20,21]. We compared the method performances over 60 movies dedicated to inference (**F1D and movie S2**). ExoDeepFinder performed better than ExoJ and ADAE GUI in terms of F1-score and Precision. For Recall, ExoDeepFinder was statistically indistinguishable from ADAE GUI, but better than ExoJ (**F1E**). Note that despite numerous efforts to run the analysis on different computers overnight and with sub-parts of the movies, ExoJ failed to produce any results for a high percentage (30-40%) of the data (**S1E**) (**see Methods**). We noticed that

85 ExoDeepFinder performances were robust over different frame rates (**S2B**) and correlated with the
86 F/F_0 SBR (**S2B**).

87 Next, we assessed ExoDeepFinder's efficiency on cells treated with different drugs that interfere with
88 secretion without retraining. We analyzed cells before and after treatment with Bafilomycin A1, a drug
89 impairing lysosomal pH homeostasis that leads to decreased exocytosis rate and additionally changes
90 cell morphology by creating stable and bright foci at the plasma membrane. ExoDeepFinder
91 performances decreased significantly after the drug treatment when compared to same cells before
92 treatment (**F2A**). However, ExoDeepFinder was still able to estimate correctly exocytosis rate and
93 produced a correct estimation of drug effect size (**F2B**) even though it was exclusively trained on
94 constitutive exocytosis events. Indeed Cohen's d predicted by ExoDeepFinder was -1.57 while ground
95 truth was d=-1.67. Similarly, ExoJ and ADAE GUI performances decreased (**S3A and C**), but contrarily
96 to ExoDeepFinder, ADAE GUI and ExoJ made wrong estimations of exocytosis rates, especially after
97 treatment (**S3B and D**). Both predicted an effect in the wrong direction (d=0.10 for ExoJ and d=0.37 for
98 ADAE GUI).

99 Additionally, we analyzed cells treated with histamine that stimulates lysosomal exocytosis[28,30].
100 Contrarily to Bafilomcyine A1, cell morphology and the aspect of individual secretory events was
101 preserved. In these conditions, we observed that ExoDeepFinder performances were not impaired
102 (**F2C**) and estimated precisely exocytosis rate as well as effect size (predicted d=0.87 while ground
103 truth d=0.88) (**F2D**). ExoJ and ADAE GUI performances were not impacted by histamine treatment
104 either (**S3E and G**). However, due to their inherent lower performances, estimated exocytosis
105 frequency and effect size were less accurate (d=0.37 for ExoJ and d=0.98 for ADAE GUI) (**S3F and H**).

106 We next detected VAMP7+ exocytosis events in another cell type (HeLa) still without re-training of
107 ExoDeepFinder. The ExoDeepFinder performances were similar good as in RPE1 cells (**F2E**), and the
108 estimated exocytosis rate was statistically indistinguishable from ground truth (**F2F**). Surprisingly, ExoJ
109 performances decreased a lot (**S4A**): the estimated exocytosis rate decreased significantly compared
110 to ground truth (**S4B**). This is surprising, because part of the ExoJ validation was performed on the
111 VAMP7-pHluorin probe in HeLa cells[22]. ADAE GUI Precision decreased slightly (**S4C**), and the predicted
112 exocytosis rate was significantly over-estimated (**S4D**).

113 Finally, we evaluated the detection of another cargo, CD63, a transmembrane protein of the
114 tetraspanin family that is used as a marker of the secretion of multi-vesicular bodies. Exocytosis events
115 in RPE1 cells were monitored with a CD63-pHluorin probe[30]. We found that ExoDeepFinder
116 performances were roughly preserved (**F2G**), and exocytosis rate was statistically indistinguishable to
117 ground truth (**F2H**). ExoJ F1-score and Recall substantially increased for this dataset but the Precision
118 value decreased (**S4E**). Note that although CD63-pHluorin was used to validate ExoJ[22], the exocytosis
119 rate predicted by ExoJ was underestimated, even if not significantly (**S4F**) due to the low number of
120 movies that were analyzable with ExoJ. Contrary, ADAE GUI F1-score and Precision decreased
121 substantially (**S4G**), and the predicted rate was significantly over-estimated compared to ground truth
122 (**S4H**).

123 In conclusion, we developed ExoDeepFinder using the U-net DeepFinder architecture, originally
124 designed for macromolecule detection in 3D cryo-electron cell tomograms. We demonstrated that
125 ExoDeepFinder, trained on 60 TIRF movies and hybrid annotations, outperformed unsupervised
126 conventional methods of exocytosis detection (**F1E**) and was more robust (**F2**). Moreover,
127 ExoDeepFinder achieved good performances even with smaller training datasets (**Table S1**). A multi-
128 class training of ExoDeepFinder increased its performance[26] (**F1C**), but may require additional work for
129 the user such as the segmentation of counter-examples events. A particular advantage of
130 ExoDeepFinder is its speed to analyze large 2D+time volume data: It takes about 30 seconds to process

131 a video of 300 x 300 x 1000 voxels with no parameter adjustments, contrary to 10 to 20 minutes
132 required with the two conventional image analysis algorithms used in our benchmark analysis that
133 additionally required manual parameter calibration. The training required 8 to 18 hours of computing
134 (once for all), depending on the desired number of epochs and the GPU performance. Importantly, we
135 endeavored to produce an user-friendly software version of ExoDeepFinder publically avalable (**see**
136 **data and software availability**). Moreover, our software allowed user to re-train the network on its
137 own data. We showed that ExoDeepFinder is capable of imitating expert annotations on experimental
138 videos. ExoDeepFinder was demonstrated to robustly perform on TIRF videos with variable
139 experimental conditions (various cargo, cell lines, microscopes, cameras, fluorophores, SBRs, etc.) It is
140 able to reliably detect exocytosis events on signals from previously unseen proteins. It can be re-
141 trained from an external dataset or fine-tuned to adapt to other target cell types or proteins. We
142 provide an open-source implementation of the ExoDeepFinder software, the manual annotated
143 dataset for training, and the trained model for inference and fine-tuning. ExoDeepFinder performances
144 also open the possibility to develop similar Deep-Learning approaches dedicated to the analysis of
145 other dynamic processes such as endocytosis or the detection of blinking spots in the context of super-
146 resolution microscopy.

147

148
149

Acknowledgments.
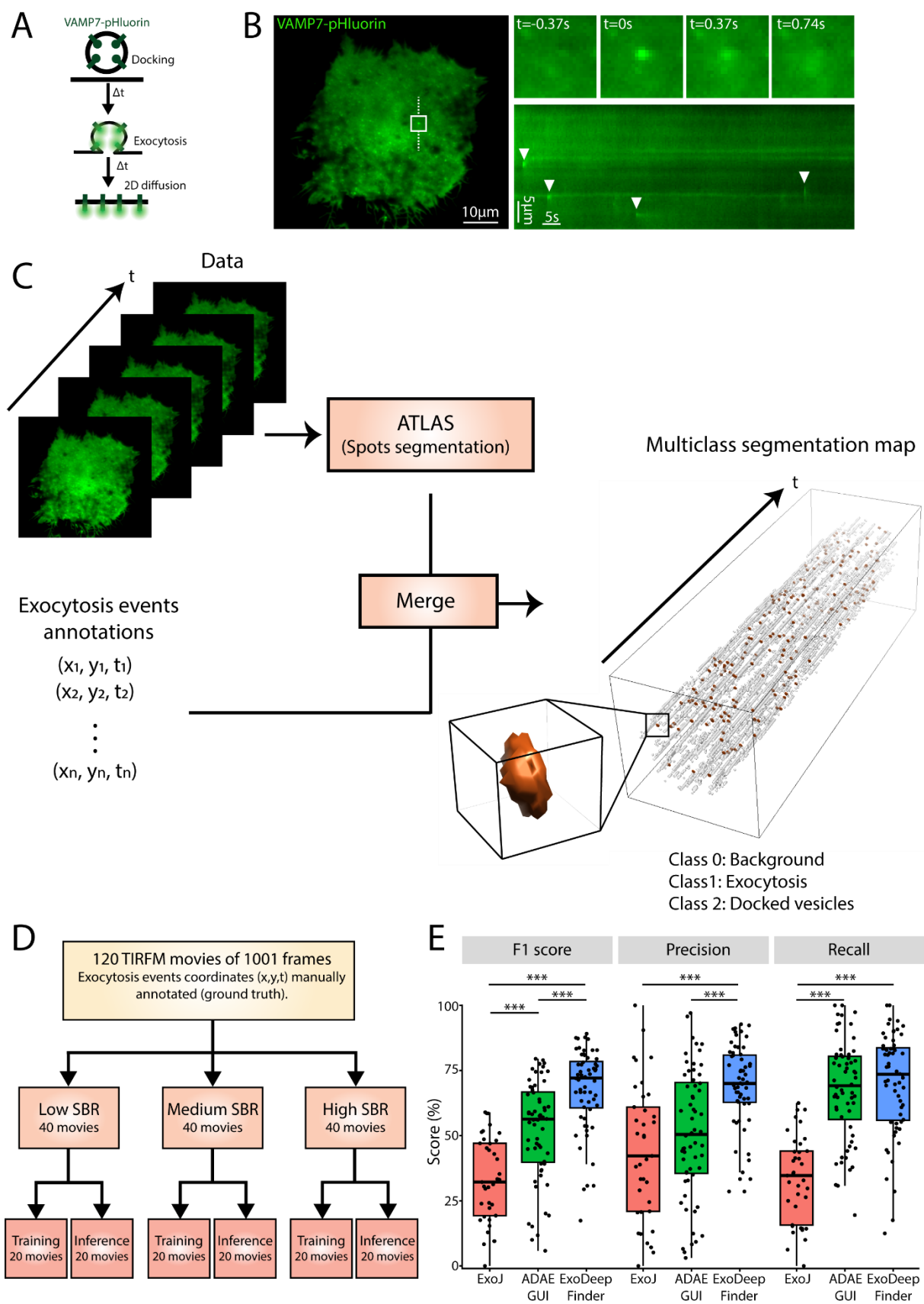
159

160

161

162

163

164

165

166

167

168

Figure 1. **A**. Schematic representation of the exocytosis of a VAMP7-pHluorin-positive vesicle: the low pH of the acidic lumen quenches the fluorescence of pHluorin. During exocytosis, protons are released and pHluorin starts to emit light. An exocytosis event is followed by the 2D diffusion of VAMP7-

172 pHluorin at the plasma membrane. **B**. TIRFM image of VAMP7-pHluorin in a transfected RPE1 cell. The
173 inset represents the field in the white square showing one exocytosis event at different time points,
174 t=0 represents the peak of the exocytosis event. A kymograph is plotted along the dashed white line
175 and arrowheads indicate several observed exocytosis events. **C**. Workflow of the data preparation for
176 ExoDeepFinder training. On the one hand, manual annotation gives the coordinates of 'ground truth'
177 exocytosis events, on the other hand, spots corresponding to docked vesicle are detected thanks to
178 the ATLAS algorithm. Both annotations are merged to produce a multiclass segmentation map. The
179 resulting spatial coordinates are converted into a 3D mask. The luminescence of an exocytosis event is
180 isotropic in the (x,y) plane and has an exponential decay in t. Therefore, we model an exocytosis event
181 as a tube with an exponentially decaying radius starting at R=4 pixels and ending at R=1 pixel, the
182 length of the tube being 3 frames in the temporal dimension as illustrated in the insight. Hence, our
183 segmentation map is composed of 3 classes: background (class 0), *bona fide* exocytosis event (class 1)
184 and docked vesicles/constant spot (class 2). **D**. Organization of the dataset. The dataset is composed
185 of 120 TIRFM movies of 1001 frames. Each movie has a manual annotation of exocytosis event
186 coordinates constituting the ground truth. The dataset is split into 3 equal subgroups according to the
187 average SBR (=F/F_0) of each movie. Then, each SBR group is randomly split into two equal sub-groups,
188 one dedicated to ExoDeepFinder training and the other one to inference *i.e.* ExoDeepFinder
189 evaluation. **E**. Comparison of ExoDeepFinder performances with ExoJ and ADAE GUI on the same
190 inference dataset of 60 movies. Significance has been evaluated with a Kruskal-Wallis test (p<0.001)
191 and pairwise comparison with a Dunn's post-hoc test with a multiple comparison Holm correction,
192 ***p<0.001 (other comparison are not significant *i.e.* p>0.05). ExoJ has less number of movies analyzed
193 (hence less total number of events) because the analysis cannot be performed for 30-40% of the data
194 (**see method**). ExoDeepFinder was trained on the total 60 movies of the training dataset (model all).

195

196

197

198

199

200

201

202

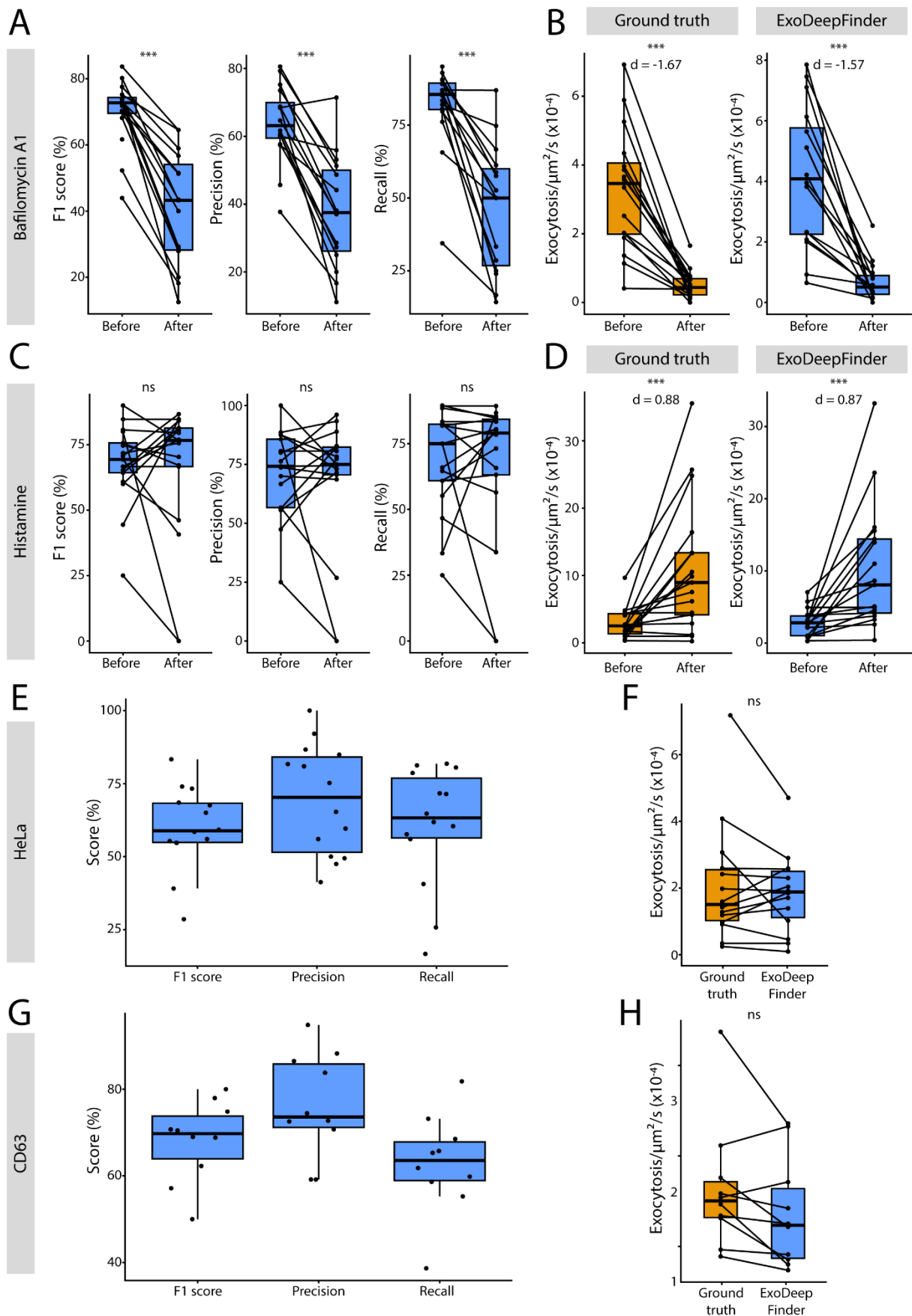203

204

205

206

207

208

209

210

Figure 2. A. ExoDeepFinder performances before and after Bafilomycin A1 (100 nM, 60 min) treatment. Note that one point is unpaired that represents a cell with no predicted events after treatment (hence,

214   F1-score, Precision and Recall cannot be defined). **B**. Exocytosis rate before and after Bafilomycin A1
215   (100 nM, 60 min) treatment measured by manual detection (ground truth) and compared to
216   ExoDeepFinder detection. In A-B, n=16 cells from three independent experiments with a total 3008
217   and 401 exocytosis events before and after drug addition, respectively, are shown. **C**. ExoDeepFinder
218   performances before and after histamine (100µM, cells immediately imaged) treatment. **D**. Exocytosis
219   rate before and after histamine (10 µM, cells immediately imaged) treatment measured by manual
220   detection (ground truth) and compared to ExoDeepFinder detection. In C-D, n = 17 cells from three
221   independent experiments with a total 2292 and 3201 exocytosis events before and after drug addition
222   respectively, are shown. **E.** ExoDeepFinder performances in VAMP7-pHluorin transfected HeLa cells. **F**.
223   Comparison of the exocytosis rate measured by manual detection (ground truth) and compared to
224   ExoDeepFinder detection. In E and F, 14 cells analyzed from a single experiment with a total of 1045
225   exocytosis events, are shown. **G**. ExoDeepFinder performances in CD63-pHluorin transfected RPE1
226   cells. **H**. Comparison of the exocytosis rate measured by manual detection (ground truth) and
227   compared to ExoDeepFinder detection. In G and H, 10 cells analyzed from a single experiment with a
228   total of 972 exocytosis events, are shown. In A-D, F and H significance has been evaluated with paired
229   Wilcoxon test, ns $p>0.05$ and ***$p<0.001$. In B and D, effect sizes are measured with the Cohen's d for
230   paired samples. In A-H, ExoDeepFinder was trained on the total 60 movies of the training dataset
231   (model all).

232

233

234

235

236

237

238

239

240

241

242

243

244

245

246

247

248

249

250

Tables

	F1-score (%)	Recall (%)	Precision (%)
All	67.64 ± 15.91	70.07 ± 19.81	68.75 ± 16.57
Subset A	54.77 ± 20.50	52.30 ± 23.02	64.65 ± 22.13
Subset B	61.68 ± 20.06	62.75 ± 23.65	65.94 ± 20.35
Subset C	63.62 ± 19.82	63.95 ± 23.68	69.60 ± 20.30
Subset D	62.67 ± 19.39	62.51 ± 23.58	69.67 ± 20.23
Subset E	64.51 ± 19.93	62.95 ± 22.96	70.96 ± 19.51
Low SBR	62.19 ± 18.83	69.91 ± 21.23	61.54 ± 22.20
Medium SBR	58.26 ± 20.22	70.05 ± 23.07	58.31 ± 24.74
High SBR	60.37 ± 21.18	58.26 ± 23.16	68.67 ± 22.70

Table 1. Performances of ExoDeepFinder for the different training datasets defined in **Table S1**. Values are mean ± SD.

References

1. Minaee, S., Boykov, Y., Porikli, F., Plaza, A., Kehtarnavaz, N., and Terzopoulos, D. (2022). Image Segmentation Using Deep Learning: A Survey. IEEE Trans. Pattern Anal. Mach. Intell. *44*, 3523–3542. https://doi.org/10.1109/TPAMI.2021.3059968.

2. Ronneberger, O., Fischer, P., and Brox, T. (2015). U-Net: Convolutional Networks for Biomedical Image Segmentation. Preprint at arXiv, https://doi.org/10.48550/arXiv.1505.04597 https://doi.org/10.48550/arXiv.1505.04597.

3. Chai, B., Efstathiou, C., Yue, H., and Draviam, V.M. (2023). Opportunities and challenges for deep learning in cell dynamics research. Trends Cell Biol., S0962-8924(23)00228-3. https://doi.org/10.1016/j.tcb.2023.10.010.

4. Pécot, T., Bouthemy, P., Boulanger, J., Chessel, A., Bardin, S., Salamero, J., and Kervrann, C. (2015). Background fluorescence estimation and vesicle segmentation in live cell imaging with conditional random fields. IEEE Trans. Image Process. Publ. IEEE Signal Process. Soc. *24*, 667–680. https://doi.org/10.1109/TIP.2014.2380178.

5. Roudot, P., Ding, L., Jaqaman, K., Kervrann, C., and Danuser, G. (2017). Piecewise-stationary motion modeling and iterative smoothing to track heterogeneous particle motions in dense environments. IEEE Trans. Image Process. Publ. IEEE Signal Process. Soc. *26*, 5395–5410. https://doi.org/10.1109/TIP.2017.2707803.

6. Pécot, T., Zengzhen, L., Boulanger, J., Salamero, J., and Kervrann, C. (2018). A quantitative approach for analyzing the spatio-temporal distribution of 3D intracellular events in fluorescence microscopy. eLife *7*, e32311. https://doi.org/10.7554/eLife.32311.

7. Newby, J.M., Schaefer, A.M., Lee, P.T., Forest, M.G., and Lai, S.K. (2018). Convolutional neural networks automate detection for tracking of submicron-scale particles in 2D and 3D. Proc. Natl. Acad. Sci. *115*, 9026–9031. https://doi.org/10.1073/pnas.1804420115.

8. Sebastian, R., Diaz, M.-E., Ayala, G., Letinic, K., Moncho-Bogani, J., and Toomre, D. (2006). Spatio-temporal analysis of constitutive exocytosis in epithelial cells. IEEE/ACM Trans. Comput. Biol. Bioinform. *3*, 17–32. https://doi.org/10.1109/TCBB.2006.11.

9. Bai, L., Wang, Y., Fan, J., Chen, Y., Ji, W., Qu, A., Xu, P., James, D.E., and Xu, T. (2007). Dissecting multiple steps of GLUT4 trafficking and identifying the sites of insulin action. Cell Metab. *5*, 47–57. https://doi.org/10.1016/j.cmet.2006.11.013.

10. Vallotton, P., James, D.E., and Hughes, W.E. (2007). Towards fully automated Identification of Vesicle-Membrane Fusion Events in TIRF Microscopy. AIP Conf. Proc. *952*, 3–10. https://doi.org/10.1063/1.2816641.

11. Huang, S., Lifshitz, L.M., Jones, C., Bellve, K.D., Standley, C., Fonseca, S., Corvera, S., Fogarty, K.E., and Czech, M.P. (2007). Insulin stimulates membrane fusion and GLUT4 accumulation in clathrin coats on adipocyte plasma membranes. Mol. Cell. Biol. *27*, 3456–3469. https://doi.org/10.1128/MCB.01719-06.

12. Mele, K., Coster, A., Burchfield, J.G., Lopez, J., James, D.E., Hughes, W.E., and Vallotton, P. (2009). Automatic identification of fusion events in TIRF microscopy image sequences. In 2009 IEEE 12th International Conference on Computer Vision Workshops, ICCV Workshops, pp. 578–584. https://doi.org/10.1109/ICCVW.2009.5457651.

317   13. Boulanger, J., Gidon, A., Kervran, C., and Salamero, J. (2010). A Patch-Based Method for
318   Repetitive and Transient Event Detection in Fluorescence Imaging. PLOS ONE 5, e13190.
319   https://doi.org/10.1371/journal.pone.0013190.

320   14. Smith, M.B., Karatekin, E., Gohlke, A., Mizuno, H., Watanabe, N., and Vavylonis, D. (2011).
321   Interactive, Computer-Assisted Tracking of Speckle Trajectories in Fluorescence Microscopy:
322   Application to Actin Polymerization and Membrane Fusion. Biophys. J. 101, 1794–1804.
323   https://doi.org/10.1016/j.bpj.2011.09.007.

324   15. Yuan, T., Lu, J., Zhang, J., Zhang, Y., and Chen, L. (2015). Spatiotemporal detection and analysis of
325   exocytosis reveal fusion "hotspots" organized by the cytoskeleton in endocrine cells. Biophys. J.
326   108, 251–260. https://doi.org/10.1016/j.bpj.2014.11.3462.

327   16. Wu, J., Xu, Y., Feng, Z., and Zheng, X. (2015). Automatically Identifying Fusion Events between
328   GLUT4 Storage Vesicles and the Plasma Membrane in TIRF Microscopy Image Sequences.
329   Comput. Math. Methods Med. 2015, 610482. https://doi.org/10.1155/2015/610482.

330   17. Basset, A., Bouthemy, P., Boulanger, J., Waharte, F., Kervrann, C., and Salamero, J. (2015).
331   Detection and estimation of membrane diffusion during exocytosis in TIRFM image sequences. In
332   2015 IEEE 12th International Symposium on Biomedical Imaging (ISBI), pp. 695–698.
333   https://doi.org/10.1109/ISBI.2015.7163968.

334   18. Basset, A., Boulanger, J., Salamero, J., Bouthemy, P., and Kervrann, C. (2015). Adaptive Spot
335   Detection With Optimal Scale Selection in Fluorescence Microscopy Images. IEEE Trans. Image
336   Process. 24, 4512–4527. https://doi.org/10.1109/TIP.2015.2450996.

337   19. Basset, A., Bouthemy, P., Boulanger, J., Waharte, F., Salamero, J., and Kervrann, C. (2017). An
338   extended model of vesicle fusion at the plasma membrane to estimate protein lateral diffusion
339   from TIRF microscopy images. BMC Bioinformatics 18, 352. https://doi.org/10.1186/s12859-017-
340   1765-y.

341   20. Urbina, F.L., Gomez, S.M., and Gupton, S.L. (2018). Spatiotemporal organization of exocytosis
342   emerges during neuronal shape change. J. Cell Biol. 217, 1113–1128.
343   https://doi.org/10.1083/jcb.201709064.

344   21. Urbina, F., and Gupton, S.L. (2021). Automated Detection and Analysis of Exocytosis. J. Vis. Exp.
345   JoVE. https://doi.org/10.3791/62400.

346   22. Liu, J., Verweij, F.J., Niel, G.V., Galli, T., Danglot, L., and Bun, P. (2024). ExoJ: an ImageJ2/Fiji
347   plugin for automated spatiotemporal detection and analysis of exocytosis. Preprint at bioRxiv,
348   https://doi.org/10.1101/2022.09.05.506585 https://doi.org/10.1101/2022.09.05.506585.

349   23. O'Shaughnessy, E.C., Lam, M., Ryken, S.E., Wiesner, T., Lukasik, K., Zuchero, J.B., Leterrier, C.,
350   Adalsteinsson, D., and Gupton, S.L. (2024). pHusion: A robust and versatile toolset for automated
351   detection and analysis of exocytosis. J. Cell Sci., jcs.261828. https://doi.org/10.1242/jcs.261828.

352   24. Li, H., Mao, Y., Yin, Z., and Xu, Y. (2017). A Hierarchical Convolutional Neural Network for vesicle
353   fusion event classification. Comput. Med. Imaging Graph. Off. J. Comput. Med. Imaging Soc. 60,
354   22–34. https://doi.org/10.1016/j.compmedimag.2017.04.003.

355   25. Martineau, M., Somasundaram, A., Grimm, J.B., Gruber, T.D., Choquet, D., Taraska, J.W., Lavis,
356   L.D., and Perrais, D. (2017). Semisynthetic fluorescent pH sensors for imaging exocytosis and
357   endocytosis. Nat. Commun. 8, 1412. https://doi.org/10.1038/s41467-017-01752-5.

26. Moebel, E., Martinez-Sanchez, A., Lamm, L., Righetto, R.D., Wietrzynski, W., Albert, S., Larivière, D., Fourmentin, E., Pfeffer, S., Ortiz, J., et al. (2021). Deep learning improves macromolecule identification in 3D cellular cryo-electron tomograms. Nat. Methods *18*, 1386–1394. https://doi.org/10.1038/s41592-021-01275-4.

27. Gubins, I., Chaillet, M.L., van der Schot, G., Veltkamp, R.C., Förster, F., Hao, Y., Wan, X., Cui, X., Zhang, F., Moebel, E., et al. (2020). SHREC 2020: Classification in cryo-electron tomograms. Comput. Graph. *91*, 279–289. https://doi.org/10.1016/j.cag.2020.07.010.

28. Lachuer, H., Le, L., Lévêque-Fort, S., Goud, B., and Schauer, K. (2023). Spatial organization of lysosomal exocytosis relies on membrane tension gradients. Proc. Natl. Acad. Sci. U. S. A. *120*, e2207425120. https://doi.org/10.1073/pnas.2207425120.

29. Jaiswal, J.K., Andrews, N.W., and Simon, S.M. (2002). Membrane proximal lysosomes are the major vesicles responsible for calcium-dependent exocytosis in nonsecretory cells. J. Cell Biol. *159*, 625–635. https://doi.org/10.1083/jcb.200208154.

30. Verweij, F.J., Bebelman, M.P., Jimenez, C.R., Garcia-Vallejo, J.J., Janssen, H., Neefjes, J., Knol, J.C., de Goeij-de Haas, R., Piersma, S.R., Baglio, S.R., et al. (2018). Quantifying exosome secretion from single cells reveals a modulatory role for GPCR signaling. J. Cell Biol. *217*, 1129–1142. https://doi.org/10.1083/jcb.201703206.